Geochemical Perspectives Letters

Noble gas incorporation into silicate glasses: implications for planetary volatile storage

H. Yang[1*], A.E. Gleason[1,2], S.N. Tkachev[3], B. Chen[4], R. Jeanloz[5], W.L. Mao[1,2]

OPEN ACCESS
doi: 10.7185/geochemlet.2105

Abstract

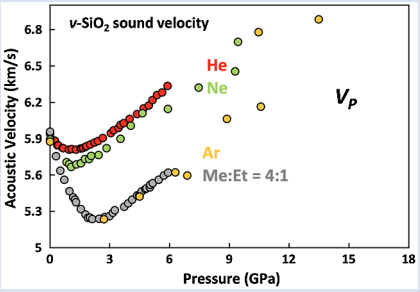

Incorporation of small molecules in silicate melts may provide an important mechanism for storing noble gases in the deep Earth, yet the means by which chemically inert noble gases enter and are retained in silica-based materials is not understood. High pressure, room temperature sound velocity measurements on silica and natural basalt glasses in different pressure-transmitting media reveal that neon enters the structure of silicate glasses and enhances their elastic strengths, whereas an ethanol-methanol mixture does not. Combined with literature data, we found the incorporation of small molecules into silica and basalt glasses is controlled by the void size distribution of the glass and size of the molecules. Pressure primarily reduces the size of noble gases, thereby increasing their solubilities in silicate melts and glasses.

Received 21 September 2020 | Accepted 6 January 2021 | Published 10 February 2021

Introduction

Radiogenic heat production generates ^{40}Ar, ^{21}Ne and ^{4}He inside Earth, and the ratios of these isotopes to non-radiogenic isotopes have been used to infer the style of mantle convection and the source of ocean island basalts (*e.g.*, Mukhopadhyay and Parai, 2019). Owing to their changing reactivity and volatility with pressure, noble gases are also useful geochemical tracers for the interior processes of planets (*e.g.*, Sanloup *et al.*, 2005). However, how these noble gases are distributed among potential geochemical reservoirs, and how they alter the physical properties of their host with increasing depth (and therefore pressure) is still unclear. The storage of noble gases in quartz, ferropericlase, and bridgmanite at high pressure has been experimentally verified (Sanloup *et al.*, 2005; Rosa *et al.*, 2020). Nevertheless, the partition coefficients of noble gases between minerals and melts are on the order of 10^{-3} (Karato, 2016), implying significant storage of noble gases in silicate melts. This deep storage could also potentially alter atmospheric composition. As silicate glasses and melts share structural similarities (Williams and Jeanloz, 1988; Morard *et al.*, 2020), with glass being the kinetically hindered state of the corresponding melt, understanding the incorporation of noble gases into silicate glasses can shed light on their storage in natural silicate melts.

Noble gases are widely used as pressure-transmitting media in high pressure diamond anvil cell experiments. These gases are chemically inactive and display relatively low mechanical strength, and thus minimise pressure gradients and deviatoric stresses in the sample chamber (Klotz *et al.*, 2009). Use of noble gases as pressure-transmitting media presumes minimal interaction with the pressurised sample, yet there have been several reports that helium penetrates into the structure of silica glass at room temperature, enhancing both its incompressibility and rigidity (Sato *et al.*, 2011; Shen *et al.*, 2011; Weigel *et al.*, 2012). Another study on basalt and enstatite glasses also indicates neon can enter their structure at high pressure (Clark *et al.*, 2016).

Void space analysis of silica could shed light on the incorporation of noble gases into its structure. Theoretical simulations of the structure of silica glass and void size analysis have provided statistics on the interstitial space (*i.e.* the largest spherical site not occupied by Si or O) that could potentially be available for incorporating noble gases (Shackelford and Masaryk, 1978; Malavasi *et al.*, 2006). However, systematic study of the high pressure solubility of these gases in silica glass has been lacking, despite a number of studies on helium (Sato *et al.*, 2011; Shen *et al.*, 2011; Weigel *et al.*, 2012).

To help clarify the mechanism of noble gas incorporation into amorphous silica and natural silicate glasses, we measured high pressure Brillouin spectra of silica and basalt glasses using different pressure-transmitting media at room temperature. The measured elastic properties of the material provide insight into the structural evolution and molecule incorporation of each glass

1. Department of Geological Sciences, Stanford University, Stanford, CA 94305, USA
2. SLAC National Accelerator Laboratory, Menlo Park, CA 94025, USA
3. Center for Advanced Radiation Sources, University of Chicago, Chicago, Illinois 60637, USA
4. Center for High Pressure Science and Technology Advanced Research, Pudong, Shanghai 201203, China
5. Earth and Planetary Sciences Department, University of California, Berkeley, CA 94720, USA
* Corresponding author (email: hyang666@stanford.edu)

with compression. Elasticity is a useful monitor of the solution process because *in situ* measurement of gas solubility is challenging at high pressure. Together with existing literature data, we provide a comprehensive review of noble gases migrating into silica glass and natural basalt glasses under pressure. We find that solubility is controlled by the atomic sizes of the noble gases relative to the size of available interstitial spaces in the silicate glasses. Pressure alters both factors, thereby affecting the solubility of noble gases and other volatile species in glasses and melts.

Results

Details on sample synthesis, compositions, and data collection can be found in the Supplementary Information. We found that the sound velocities of silica glass depend on the pressure-transmitting medium (Fig. 1). We observed a drop in both compressional and shear velocities when increasing pressure between 1 and 3 GPa, followed by a slightly increasing or nearly unchanged velocity at higher pressures (Fig. 1). Silicate glasses with natural compositions share a similar framework structure with silica glass, and their velocity drop upon initial compression was also documented in other polymerised silicate glasses, such as basalt, jadeite and albite glasses (Liu and Lin, 2014; Sakamaki *et al.*, 2014). In contrast, depolymerised glasses like diopside or enstatite glass do not show a decreasing trend, but rather an almost pressure-independent velocity (Sanchez-Valle and Bass, 2010; Liu and Lin, 2014; Sakamaki *et al.*, 2014). These observations can be explained by the flexibility of SiO_4 tetrahedra networks. In the low pressure range, below 3 GPa, the SiO_4 tetrahedra in the glass rotate into the void space to form a high-density structure (Clark *et al.*, 2016). The rotation does not involve substantial compression of the interatomic bonds, so the elastic moduli of the material remain largely unaltered. Therefore, the velocities, given by the square root of the ratio of the moduli and density, decrease during this stage. However, after the void space is filled, tetrahedral rotation is replaced by the interatomic bond shortening, and the sound velocities then increase under compression (Clark *et al.*, 2016). Depolymerised silicate glasses, which contain larger 'modifier' cations like Mg^{2+}, Na^{2+} or Ca^{2+}, have less void space and

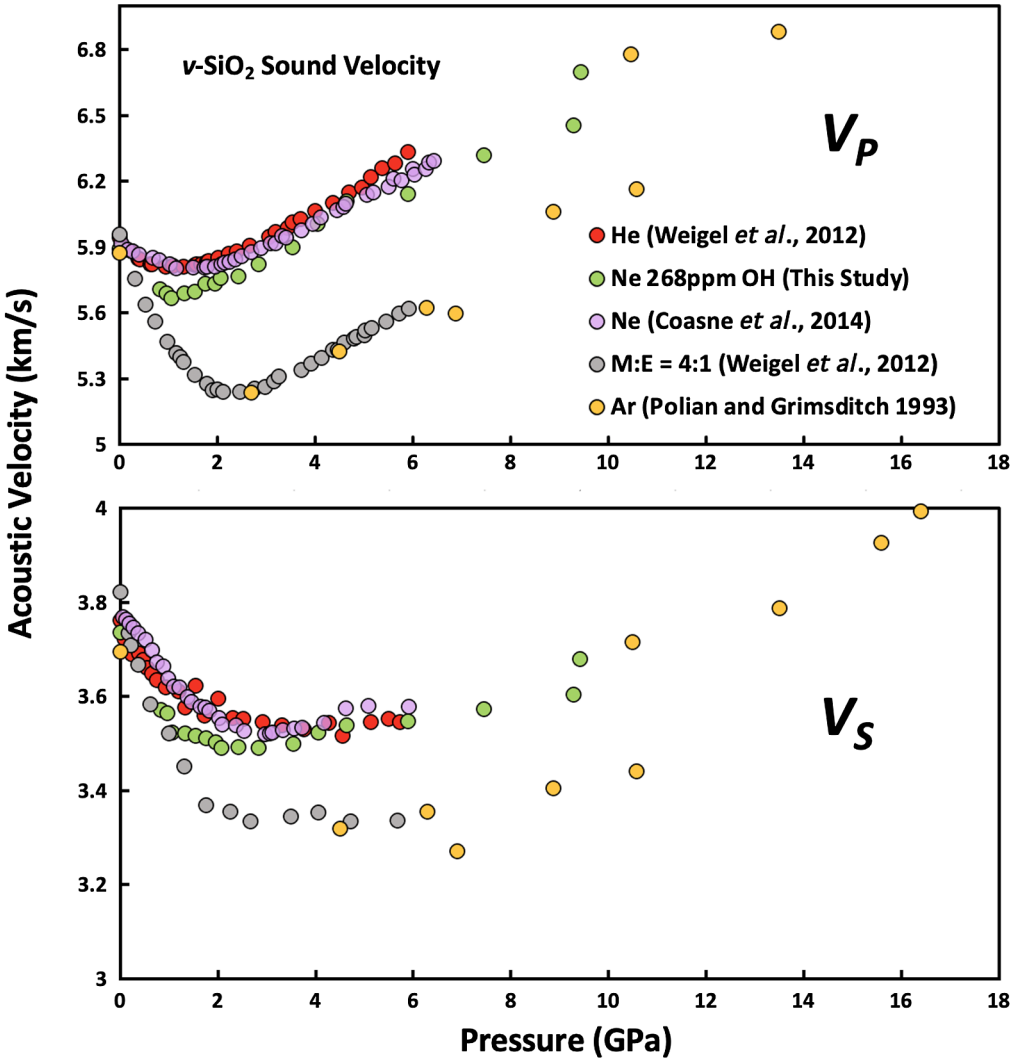

Figure 1 Sound velocities of vitreous silica under high pressure in different pressure media. M-E represents 4 : 1 Methanol-Ethanol mixture. Errors of the velocities are estimated from statistical uncertainties arising from the peak fitting. Typical errors are less than 1.5 % and smaller than the size of the symbols. For both the V_P and V_S of silica in different noble gas media, we found a consistent trend for the acoustic velocities — He > Ne > Ar ≈ M-E. The abnormal velocity minimum at around 2–5 GPa can be attributed to the rearrangement of SiO_4 tetrahedra in the vitreous silica structure (Clark *et al.*, 2016).

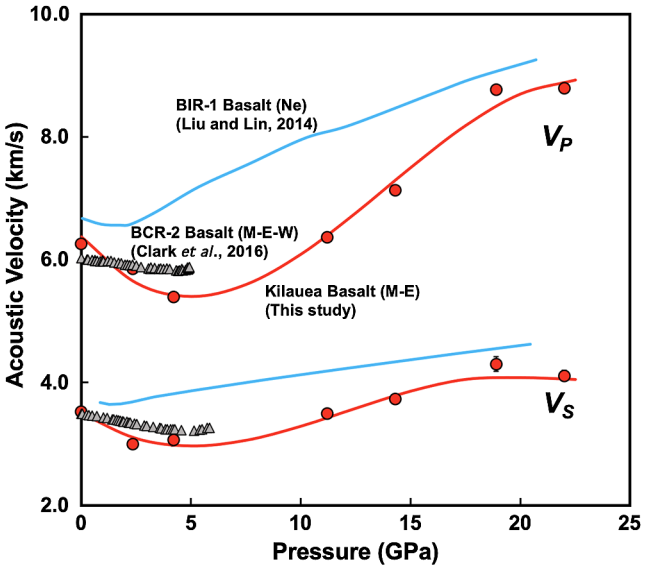

Figure 2 Sound velocities of basalt glasses at high pressure. M-E-W: 16:3:1 Methanol-Ethanol-Water mixture, M-E: 4:1 Methanol-Ethanol mixture. Errors of the velocities are estimated from statistical uncertainties arising from the peak fitting. Error bars smaller than the symbols plotted are not shown. Although the three basalt glasses have slightly different compositions, their degrees of polymerisation (NBO/T = 0.6, 0.9 and 0.8 for BCR-2, BIR-1 and KB, respectively) are quite similar (BIR-1, blue coloured line, Liu and Lin, 2014; BCR-2, triangular points, Clark *et al.*, 2016). The extents of the velocity drops are very different among the glasses. We observed that BIR-1 has a 2 % drop for both V_P and V_S, BCR-2 has a 2.8 % drop for V_P and a 7.2 % drop for V_S, while KB in M-E has a 14 % drop for both V_P and V_S. We attribute this variation to be mostly due to the different pressure media used. H_2O and Ne have a relatively small molecule size that can possibly penetrate into the structure of silicate glass and make it stiffer (Figs. 3, S-4).

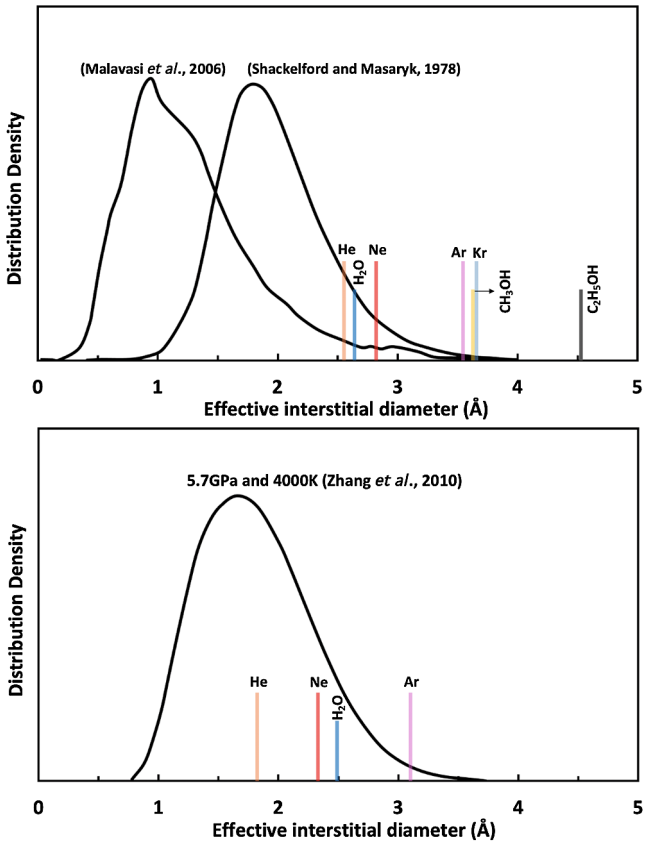

Figure 3 Void size distribution of SiO_2 and molecular size of common pressure media at ambient condition and high pressure. **Top panel:** Molecular size data at ambient conditions were adapted from Reid *et al.* (1987). **Bottom panel:** High pressure molecule sizes were calculated using equations of state (He: Loubeyre *et al.*, 1993; Ne: Dewaele *et al.*, 2008; Ar: Ross *et al.*, 1986, H_2O: Yoshimura *et al.*, 2006).

consequently less flexibility. The densification may also involve some chemical bond shortening and lead to the unchanged velocity profile with increasing pressure.

For basalt glasses, sound velocities at high pressure are also influenced by the pressure media (Fig. 2). The BIR-1 sample has higher velocities in a neon medium, as compared with basalt in M-E and M-E-W (methanol: ethanol: water = 16:3:1); it also has an earlier transition pressure at which the velocities start to increase. Comparing the M-E and M-E-W cases, we see that water seems to lower the decreasing slope below 5 GPa, but it does not change the transition point for the change in velocity trends (Fig. 2).

Discussion

Sound velocity data for amorphous materials can be very useful to calculate their density at high pressure (Zha *et al.*, 1994). However, this method would fail if pressure media penetrates the sample (Weigel *et al.*, 2012). We calculated the *P-V* curve from velocities observed in different media and used this to examine whether incorporation of pressure media occurred in our experiments (see Supplementary Information for details). Neon and helium seem also able to penetrate into the silica structure while water and methanol molecules seem also to be able to penetrate into basalt glasses (Fig. S-3).

We compared the molecular size of the pressure media with the size of the interstitial space in the silica structure (Figs. 3, S-4). At ambient conditions, the sizes of helium, neon and water molecules are smaller than some voids in the silica structure. At higher pressures, the void size distribution generally shifts to a smaller volume, but the peak position moves only slightly and is still larger than 1.75 Å. On the other hand, the sizes of highly compressible gases decrease dramatically with increasing pressure, especially for helium and neon (Fig. S-4). These results indicate that helium and neon elevate the elastic stiffness of silica by supporting the structure in the void space, while molecules larger than argon are too big to be incorporated into silica and do not show this effect. Pressure makes these atoms smaller, enhancing the solubility of neon and helium into silica (Fig. 3). Although argon also becomes smaller at high pressure, it is still larger than most of the voids in silica. Its solubility is limited and does not influence the elastic properties significantly (Fig. 1).

Our measurements do not provide solubility values, but by comparing the gas and non-gas experiments we can make an estimate of this parameter (Sato *et al.*, 2011) (Fig. S-3). In Figure 4, the upper limit is constrained by the maximum available space in the silica structure. This space is calculated as the volume difference between normal silica and the ultra-dense six-coordinated silica extropolated to lower pressure. On the other hand, the lower limit is given by the difference between gas and non-gas curves, assuming the 'expansion' should wholly or partly come from the volume of gas in the structure. Since the partial volume of a component in a mixture is smaller than the volume on its own (Bajgain *et al.*, 2015), the real solubility should be higher than the lower limit here.

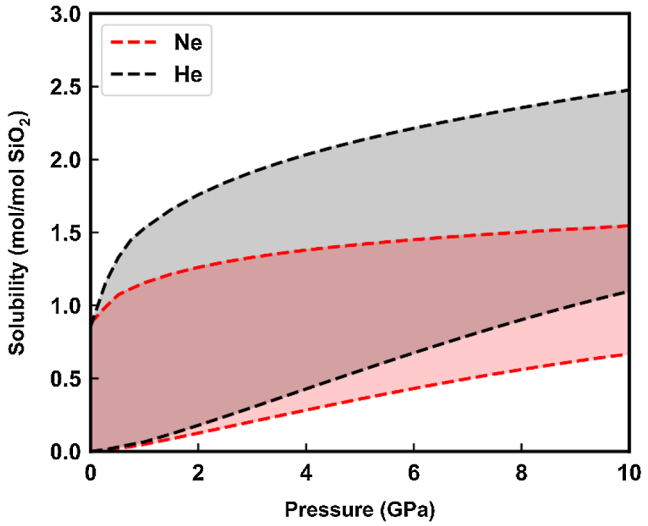

Figure 4 Solubility of neon and helium in vitreous silica at high pressure. The two lines for each medium represent upper limit and lower limits, respectively. The lower and upper limits were estimated by $(V_{rigid} - V_{normal})/V_{gas}$ and $(V_{rigid} - V_{sixfold})/V_{gas}$, respectively, where V_{rigid} and V_{normal} represent the molar volume of SiO_2 glass in noble gas media and non-gas media conditions, accordingly; V_{gas} – the molar volume of noble gas; $V_{sixfold}$ – the molar volume of six-fold-coordinated SiO_2 glass (Sato *et al.*, 2011). We do not have an accurate determination of volume of silica in Ne, instead we assume the volume change under pressure is same as the He case, as similar volume curves were suggested by integration method (Fig. S-3).

Basalt glass is compositionally more complex than silica glass with the addition of other cations. These cations can be classified into two categories: the network formers like Ti, Al and network modifiers like Mg, Ca, Na and K. The two sets of cations have distinct effects on gas solubility. Network modifiers tend to form bonds between the bridging SiO_4 tetrahedra and lower the volume of void space. Their negative correlation with noble gas solubility has been experimentally observed (Tournour and Shelby, 2008a,b). On the other hand, network formers, which reside in the Si site, seem to have less of an influence on gas solubility.

Geochemical Implications

The geometrical packing and coordination of atoms in silicate melts and glasses are similar at ambient and high pressure conditions based on experimental observations (Williams and Jeanloz, 1988; Morard *et al.*, 2020). Hence, the void space distribution in melt structure is likely to be comparable and our results here support significant solubility of helium and neon in high pressure silicate melts (Fig. 3). Furthermore, the partition coefficients between minerals and melts for noble gases are in the order of 10^{-3} (Karato, 2016). It is expected silicate melts should be an important host for noble gases. He and Ne are the 2nd and 5th most abundant elements in the solar system (Palme *et al.*, 2014). For $^{3}He/^{4}He$ and $^{20,21}Ne/^{22}Ne$ isotopic ratios, the discrepancy of upper mantle material value from the atmospheric value has been a hot topic in geochemistry (*e.g.*, Bekaert *et al.*, 2019; Mukhopadhyay and Parai, 2019). Most answers to this question require a deep primordial reservoir which has unique geochemical features and survives mantle convection for the last 4.5 billion years. It has been noticed that some patches of partially molten rock might exist at the core mantle boundary (*e.g.*, Wen *et al.*, 2001). These melts may be able to host large amounts of noble gases like helium and neon with primordial and less radiogenic features. Other than the core-mantle boundary, partial melting may also occur at the top of the lower mantle due to dehydration melting (Fu *et al.*, 2019). These layers might be perturbed by mantle convection more often and host noble gases with more radiogenic features. Therefore, the observed difference in noble gases ratios in OIBs and MORBs could be possibly due to sampling different melt reservoirs for noble gases. The storage of helium or neon discussed here reaches conditions beyond the range of this experiment, and due to the complex coordination environment change of silicon at higher pressures (Wang *et al.*, 2014), and the high temperature conditions in deep Earth, directly applying our results to these conditions may not be suitable. However, the mechanism revealed in this study and previous studies (Clark *et al.*, 2016; Sato *et al.*, 2011; Weigel *et al.*, 2012) (*i.e.* availability of interstitial void to compressed noble gases) is still valid and future structure simulation and void space analysis of heated silica/basalt glass at high pressures is needed. Geodynamic simulations are also needed to better estimate the degree of mixing during these processes.

Noble gas-silicate interaction may also have important implications for the composition of the atmospheres of other planetary bodies like Jupiter. It is found that the abundances of helium and neon in Jupiter's atmosphere are significantly lower than other noble gases, when compared to solar composition (Fortney, 2010). Our results suggest that this discrepancy could be related to interior processes in the planet, which account for the 'missing' helium and neon. Forming a He-Ne-silicate composite at Jupiter's rocky core could be a viable option to lower the fraction of He and Ne in its atmosphere. Whether such a mechanism could explain the deficit of neon and helium in Jupiter's atmosphere requires further experimental and computational work. Our study demonstrates the controlling factors for noble gas solubility in a silicate melt are the noble gas size compared to void size, indicating that data on the structure of silicate melts with natural compositions at higher *P-T* is crucially needed in order to estimate the storage capacity of noble gases in deep planetary interiors.

Acknowledgements

We appreciate constructive comments from two anonymous reviewers. AEG and WM acknowledge support from NSF Geophysics (EAR0738873). RJ acknowledges support from UC CMEC. Work was performed at GeoSoilEnviroCARS which is supported by NSF (EAR – 1634415) and DOE (DE-FG02-94ER14466). Use of the COMPRES-GSECARS gas loading system was supported by COMPRES under NSF (EAR -1606856) and GSECARS. The Advanced Photon Source is operated for the DOE Office of Science by Argonne National Laboratory (DE-AC02-06CH11357).

Editor: Anat Shahar

Additional Information

Supplementary Information accompanies this letter at https://www.geochemicalperspectivesletters.org/article2105.

Cite this letter as: Yang, H., Gleason, A.E., Tkachev, S.N., Chen, B., Jeanloz, R., Mao, W.L. (2021) Noble gas incorporation into silicate glasses: implications for planetary volatile storage. *Geochem. Persp. Let.* 17, 1–5.

References

Bajgain, S., Ghosh, D.B., Karki, B.B. (2015) Structure and density of basaltic melts at mantle conditions from first-principles simulations. *Nature Communications* 6, 1–7.

Bekaert, D.V., Broadley, M.W., Caracausi, A., Marty, B. (2019) Novel insights into the degassing history of Earth's mantle from high precision noble gas analysis of magmatic gas. *Earth and Planetary Science Letters* 525, 115766.

Clark, A.N., Lesher, C.E., Jacobsen, S.D., Wang, Y. (2016) Anomalous density and elastic properties of basalt at high pressure: Reevaluating of the effect of melt fraction on seismic velocity in the Earth's crust and upper mantle. *Journal of Geophysical Research: Solid Earth* 121, 4232–4248.

Coasne, B., Weigel, C., Polian, A., Kint, M., Rouquette, J., Haines, J., Foret, M., Vacher, R., Rufflé, B. (2014) Poroelastic Theory Applied to the Adsorption-Induced Deformation of Vitreous Silica. *The Journal of Physical Chemistry B* 118, 14519–14525.

Dewaele, A., Datchi, F., Loubeyre, P., Mezouar, M. (2008) High pressure–high temperature equations of state of neon and diamond. *Physical Review B* 77, 094106.

Fortney, J. (2010) Peering into Jupiter. *Physics* 3, 26.

Fu, S., Yang, J., Karato, S., Vasiliev, A., Presniakov, M. Yu., Gavrilliuk, A.G., Ivanova, A.G., Hauri, E.H., Okuchi, T., Purevjav, N., Lin, J. (2019) Water Concentration in Single-Crystal (Al,Fe)-Bearing Bridgmanite Grown From the Hydrous Melt: Implications for Dehydration Melting at the Topmost Lower Mantle. *Geophysical Research Letters* 46, 10346–10357.

Karato, S. (2016) Physical basis of trace element partitioning: A review. *American Mineralogist* 101, 2577–2593.

Klotz, S., Chervin, J.C., Munsch, P., Lemarchand, G. (2009) Hydrostatic limits of 11 pressure transmitting media. *Journal of Physics D Applied Physics* 42, 075413.

Liu, J., Lin, J.-F. (2014) Abnormal acoustic wave velocities in basaltic and (Fe,Al)-bearing silicate glasses at high pressures. *Geophysical Research Letters* 41, 8832–8839.

Loubeyre, P., LeToullec, R., Pinceaux, J.P., Mao, H.K., Hu, J., Hemley, R.J. (1993) Equation of state and phase diagram of solid 4He from single-crystal x-ray diffraction over a large P-T domain. *Physical Review Letters* 71, 2272–2275.

Malavasi, G., Menziani, M.C., Pedone, A., Segre, U. (2006) Void size distribution in MD-modelled silica glass structures. *Journal of Non-Crystalline Solids* 352, 285–296.

Morard, G., Hernandez, J.-A., Guarguaglini, M., Bolis, R., Benuzzi-Mounaix, A., Vinci, T., Fiquet, G., Baron, M.A., Shim, S.H., Ko, B., Gleason, A.E., Mao, W.L., Alonso-Mori, R., Lee, H.J., Nagler, B., Galtier, E., Sokaras, D., Glenzer, S.H., Andrault, D., Garbarino, G., Mezouar, M., Schuster, A.K., Ravasio, A. (2020) In situ X-ray diffraction of silicate liquids and glasses under dynamic and static compression to megabar pressures. *Proceedings of the National Academy of Sciences* 117, 11981–11986.

Mukhopadhyay, S., Parai, R. (2019) Noble Gases: A Record of Earth's Evolution and Mantle Dynamics. *Annual Review of Earth and Planetary Sciences* 47, 389–419.

Palme, H., Lodders, K., Jones, A. (2014) 2.2 – Solar System Abundances of the Elements. In: Holland, H.D., Turekian, K.K. (Eds.) *Treatise on Geochemistry*. Second Edition, Elsevier, Oxford, 15–36, doi: 10.1016/B978-0-08-095975-7.00118-2.

Polian, A., Grimsditch, M. (1993) Sound velocities and refractive index of densified α-SiO_2 to 25 GPa. *Physical Review B* 47, 13979–13982.

Reid, R.C., Prausnitz, J.M., Poling, B.E. (1987) The properties of gases and liquids. McGraw Hill Book Co., New York, NY.

Rosa, A.D., Bouhifd, M.A., Morard, G., Briggs, R., Garbarino, G., Irifune, T., Mathon, O., Pascarelli, S. (2020) Krypton storage capacity of the Earth's lower mantle. *Earth and Planetary Science Letters* 532, 116032.

Ross, M., Mao, H.K., Bell, P.M., Xu, J.A. (1986) The equation of state of dense argon: A comparison of shock and static studies. *The Journal of Chemical Physics* 85, 1028–1033.

Sakamaki, T., Kono, Y., Wang, Y., Park, C., Yu, T., Jing, Z., Shen, G. (2014) Contrasting sound velocity and intermediate-range structural order between polymerized and depolymerized silicate glasses under pressure. *Earth and Planetary Science Letters* 391, 288–295.

Sanchez-Valle, C., Bass, J.D. (2010) Elasticity and pressure-induced structural changes in vitreous MgSiO3-enstatite to lower mantle pressures. *Earth and Planetary Science Letters* 295, 523–530.

Sanloup, C., Schmidt, B.C., Perez, E.M.C., Jambon, A., Gregoryanz, E., Mezouar, M. (2005) Retention of Xenon in Quartz and Earth's Missing Xenon. *Science. American Association for the Advancement of Science* 310, 1174–1177.

Sato, T., Funamori, N., Yagi, T. (2011) Helium penetrates into silica glass and reduces its compressibility. *Nature Communications* 2, 345.

Shackelford, J.F., Masaryk, J.S. (1978) The interstitial structure of vitreous silica. *Journal of Non-Crystalline Solids* 30, 127–134.

Shen, G., Mei, Q., Prakapenka, V.B., Lazor, P., Sinogeikin, S., Meng, Y., Park, C. (2011) Effect of helium on structure and compression behavior of SiO2 glass. *Proceedings of the National Academy of Sciences* 108, 6004–6007.

Tournour, C.C., Shelby, J.E. (2008a) Neon solubility in silicate glasses and melts. *Physics and Chemistry of Glasses* 49, 8.

Tournour, C.C., Shelby, J.E. (2008b) Helium solubility in alkali silicate glasses and melts. *Physics and Chemistry of Glasses – European Journal of Glass Science and Technology Part B* 49, 207–215.

Wang, Y., Sakamaki, T., Skinner, L.B., Jing, Z., Yu, T., Kono, Y., Park, C., Shen, G., Rivers, M.L., Sutton, S.R. (2014) Atomistic insight into viscosity and density of silicate melts under pressure. *Nature Communications* 5, 3241.

Weigel, C., Polian, A., Kint, M., Rufflé, B., Foret, M., Vacher, R. (2012) Vitreous Silica Distends in Helium Gas: Acoustic Versus Static Compressibilities. *Physical Review Letters* 109, 245504.

Wen, L., Silver, P.G., James, D.E., Kuehnel, R. (2001) Seismic evidence for a thermochemical boundary at the base of the Earth's mantle. *Earth and Planetary Science Letters* 189, 141–153.

Williams, Q., Jeanloz, R. (1988) Spectroscopic Evidence for Pressure-Induced Coordination Changes in Silicate Glasses and Melts. *Science* 239, 902–905.

Yoshimura, Y., Stewart, S.T., Somayazulu, M., Mao, H., Hemley, R.J. (2006) High-pressure x-ray diffraction and Raman spectroscopy of ice VIII. *The Journal of Chemical Physics* 124, 024502.

Zha, C., Hemley, R.J., Mao, H., Duffy, T.S., Meade, C. (1994) Acoustic velocities and refractive index of SiO2 glass to 57.5 GPa by Brillouin scattering. *Physical Review B* 50, 13105–13112.

Zhang, C., Duan, Z., Li, M. (2010) Interstitial voids in silica melts and implication for argon solubility under high pressures. *Geochimica et Cosmochimica Acta* 74, 4140–4149.

Geochemical Perspectives Letters

Noble gas incorporation into silicate glasses: implications for planetary volatile storage

H. Yang, A.E. Gleason, S.N. Tkachev, B. Chen, R. Jeanloz, W.L. Mao

Supplementary Information

The Supplementary Information includes:

- Sample Preparation
- Brillouin Spectroscopy Measurements
- Volume Compression Curve Calculation
- Tables S-1 and S-2
- Figures S-1 to S-4
- Supplementary Information References

Sample Preparation

High-purity silica glass was synthesised at Corning Inc. by chemical vapor deposition and was annealed at 985 °C for 1500 hours. Its OH content was determined by FTIR spectroscopy to be 268 (± 7) ppm. Details of the determination of OH content are reported elsewhere (Clark *et al.*, 2014).

Natural Kilauea basalt glass was collected at the Kilauea volcano, Hawaii. The natural sample was prepared by grinding a kilogram sample into a powder and melting at 1540 °C under a nitrogen atmosphere. Two heating-quenching cycles in a furnace ensured a uniform amorphous state (Jochum *et al.*, 2000). X-ray diffraction of the samples after polishing and loading showed no crystalline phases. Chemical analysis of sample was conducted using Electron Probe Micro Analysis, and results are listed in Table S-1.

The synthesised samples were double-sided polished to ~30 um in thickness and loaded into a 200 μm diameter sample chamber drilled into a pre-indented rhenium gasket that was compressed between a pair of 400 μm flat diamond anvils. Ruby spheres were also loaded in the chamber to calibrate pressure. For silica glass, neon was loaded as the pressure medium using the gas loading system at GSECARS, Argonne National Laboratory (ANL) (Rivers *et al.*, 2008). For basalt glass, a methanol-ethanol mixture (M-E mixture) with a 4:1 ratio was used as the pressure medium.

Brillouin Spectroscopy Measurements

Brillouin scattering was performed using two different systems: (1) at the Advanced Light Source, Lawrence Berkeley National Laboratory, and (2) the Advanced Photon Source, Argonne National Laboratory. Brillouin spectra were collected up to 10 GPa for Silica glass in neon, and up to 22 GPa for basalt glass in a M-E mixture at beamline 13-BMD, GSECARS, ANL (Sinogeikin *et al.*, 2006) (Figs.1 and S-1). All measurements were made on compression at room temperature, and at each pressure samples were held for 30 minutes to stabilise pressure before data collection. Both Brillouin systems used a solid-state 532nm laser, and a six-pass tandem Fabry-Perot Interferometer along with a photomultiplier tube. Typical Brillouin spectra collection times were 15 to 30 minutes. Symmetric platelet geometry was used in the measurement to cancel the refractive-index correction in calculating velocities (Whitfield *et al.*, 1976). The *P*- and *S*-wave velocities were derived from the frequency shifts of the incident photons in the Brillouin spectra:

$$V = \frac{\Delta\nu \cdot \lambda}{2sin\frac{\theta}{2}} , \qquad \text{Eq. S-1}$$

where V is the acoustic wave velocity, $\boldsymbol{\Delta\nu}$ is the frequency shift, $\boldsymbol{\lambda}$ is the wavelength of the laser, and θ is the angle between the incident and scattered light. Uncertainties in the velocities were estimated from fitting results for the phonon peak positions (Table S-2).

Volume Compression Curve Calculation

The isentropic bulk modulus K_S can be derived from the velocities, and is related to the derivative of pressure with respect to density:

$$K_S = \rho\left(\frac{\partial P}{\partial \rho}\right)_S = \rho\left(v_P^2 - \frac{4}{3}v_s^2\right) \quad \text{Eq. S-2}$$

Correction from isentropic to isothermal conditions is small at room temperature ($K_S = K_T\,(1 + agT)$, with the product of thermal expansion coefficient a, Grüneisen parameter g and temperature T, being less than 10^{-2}). Therefore, integration of (2) could be used to calculate the volume decrease of the glasses under static compression (subscript T indicates isothermal conditions):

$$\frac{V}{V_0} = \left(\frac{\rho}{\rho_0}\right)_T^{-1} = \left(1 + \frac{1}{\rho_0}\int_{P_0}^{P} \frac{dP}{v_P^2 - \frac{4}{3}v_s^2}\right)_T^{-1} \quad \text{Eq. S-3}$$

except for two significant effects. First, Eq. S-3 ignores any volume change associated with changes in glass structure under compression (measured velocities of crystalline samples can similarly be integrated as a function of pressure, and also do not include the volume change across any crystal-structural phase transition; the volume change on transformation is instead an unknown integration constant). This effect implies that the glass sample should actually undergo greater volume compression than predicted by Eq. S-3, especially as there can in principle be dispersion between the elastic response at Brillouin frequencies and the quasi-static response under isothermal compression.

Second, Eq. S-3 ignores the possibility that the sample is an open system, in that noble gas (pressure medium) is permeating into the glass structure. In this case, we can think of the glass as being a porous medium, with noble gas filling the structural void spaces represented by porosity (*e.g.*, Weigel *et al.*, 2012). If the glass structure can be treated as rigid, filling empty pores is expected to increase the velocities of the medium; in detail, the relationship between volume compression and measured velocities is complex, however, due to potentially competing effects of structural rearrangement and void filling.

Applying the integrated Eq. S-3 to the Brillouin results does indeed produce larger volumes (*i.e.* less compression) as compared with isothermal compression measurements by optical and x-ray tomographic methods for silica and basalt glasses (Fig. S-3). This implies that the glasses undergo structural rearrangement on compression, as expected for instance due to rotation of SiO_4 tetrahedra into void spaces. The effect is relatively small for Silica glass compressed in M-E, however, and the Brillouin measurements document an additional stiffening (larger volumes at high pressure) when Ne or He are used as pressure media. Similarly, the basalt glass in Ne exhibits extra stiffening in the Brillouin velocities relative to static compression in M-E-W. In both cases, we attribute this additional stiffening (higher Brillouin velocities), as compared with M-E, to the incorporation of Ne or He into the glass structure.

Supplementary Tables

Table S-1 Composition of Kilauea Basalt sample from Electron Probe Microanalysis (weight %). The compositions of two other basaltic glasses discussed in the text were also listed for comparison. Abbreviations: KB, Kilauea Basalt; BIR-1, Icelandic Basalt; BCR-2, Columbia River Basalt. NBO/T for KB, BIR-1, and BCR-2 are 0.8, 0.9, and 0.6, respectively. Slight differences among the compositions of these basalt glasses are unlikely to significantly affect the pressure dependences or transition points for the velocities.

Oxide	KB, This study	BIR-1	BCR-2
SiO_2	49.67	47.96	54.1
TiO_2	2.91	0.96	2.26
Al_2O_3	13.49	15.5	13.5
FeO	14.24	10.2	12.4
MnO	0.18	0.175	0.196
MgO	5.94	9.7	3.59
CaO	9.72	13.3	7.12
Na_2O	2.56	1.82	3.16
K_2O	0.69	0.03	1.79

Table S-2 Experimental sound velocity data measured by Brillouin Spectroscopy. A Lorentz function was used to fit the peak and the uncertainties in the velocities were estimated from the fitting results of the phonon peak positions.

Sample	Pressure (GPa)	V_S (km/s)	Uncertainty	V_P (km/s)	Uncertainty
Kilauea basalt glass	0.0	3.53	0.03	6.26	0.03
Kilauea basalt glass	2.4	3.00	0.07	5.85	0.03
Kilauea basalt glass	4.2	3.07	0.11	5.39	0.04
Kilauea basalt glass	11.2	3.49	0.07	6.36	0.03
Kilauea basalt glass	14.3	3.74	0.06	7.13	0.02
Kilauea basalt glass	18.9	4.30	0.12	8.77	0.03
Kilauea basalt glass	22.0	4.11	0.09	8.79	0.04
Kilauea basalt glass	21.3[a]	4.27	0.16	8.91	0.06
Kilauea basalt glass	18.4[a]	4.28	0.08	8.22	0.26
Kilauea basalt glass	16.7[a]	4.04	0.15	8.23	0.04
Kilauea basalt glass	14.8[a]	3.98	0.11	7.60	0.17
Kilauea basalt glass	13.2[a]	3.94	0.11	7.29	0.06
Kilauea basalt glass	11.3[a]	3.77	0.09	7.01	0.03
Kilauea basalt glass	5.9[a]			6.87	0.03
Kilauea basalt glass	3.5[a]			6.54	0.06
Kilauea basalt glass	2.4[a]			6.38	0.06
Silica glass	0.0	3.74	0.02	5.89	0.03
Silica glass	0.8	3.57	0.02	5.71	0.03
Silica glass	1.0	3.56	0.02	5.69	0.03
Silica glass	1.1	3.52	0.01	5.68	0.02
Silica glass	1.3	3.52	0.02	5.69	0.03
Silica glass	1.5	3.52	0.03	5.70	0.02
Silica glass	1.8	3.51	0.03	5.73	0.03
Silica glass	2.0	3.50	0.03	5.74	0.02
Silica glass	2.1	3.49	0.02	5.76	0.03
Silica glass	2.8	3.49	0.03	5.83	0.04
Silica glass	3.5	3.50	0.04	5.91	0.04
Silica glass	4.1	3.52	0.02	6.01	0.03
Silica glass	4.6	3.54	0.02	6.12	0.03
Silica glass	5.9	3.55	0.02	6.15	0.03
Silica glass	7.4	3.57	0.02	6.32	0.04
Silica glass	9.3	3.60	0.02	6.46	0.03
Silica glass	9.4	3.68	0.03	6.71	0.03
Silica glass	10.5			7.25	0.02

[a] data collected during the decompression run.

Supplementary Figures

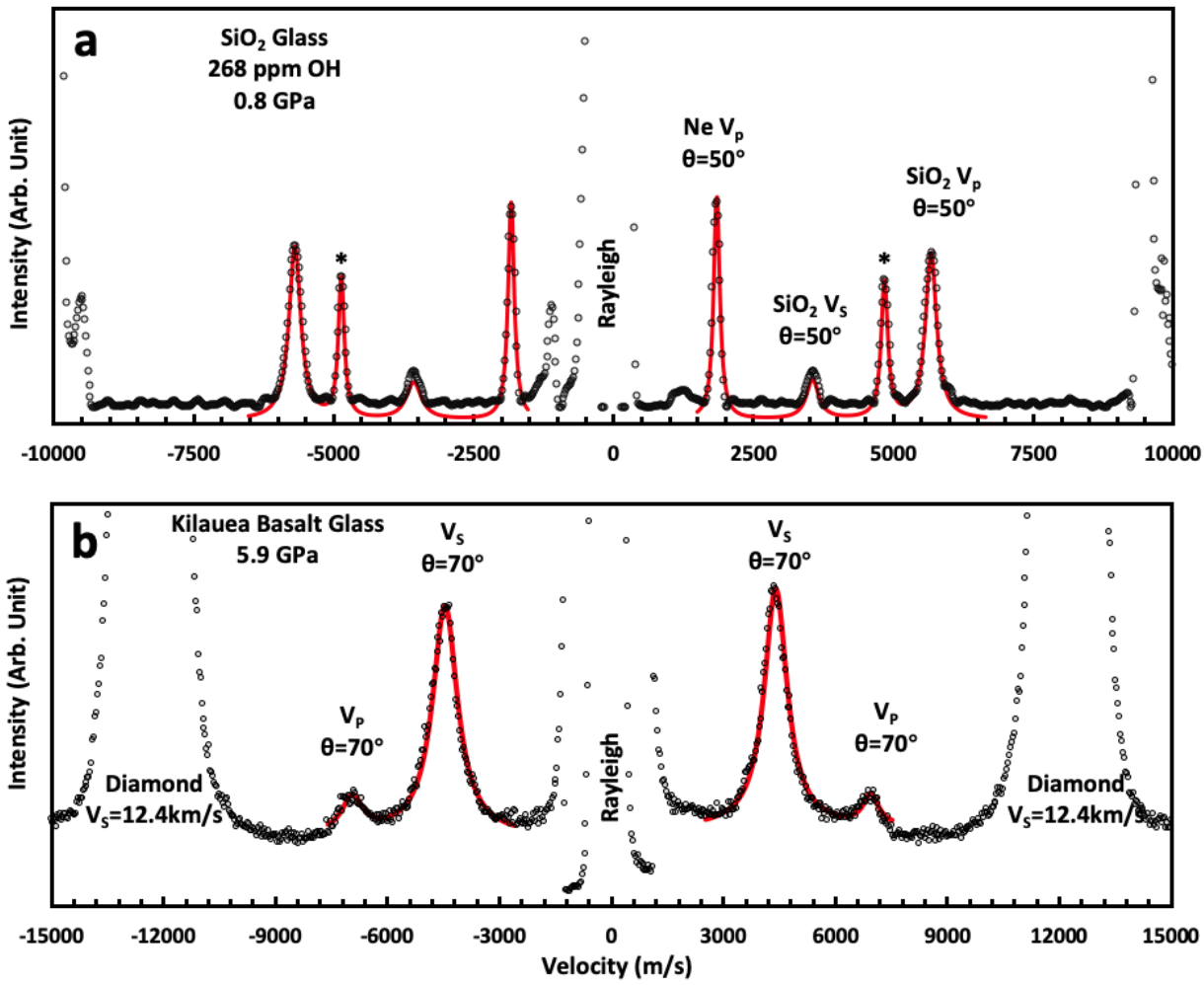

Figure S-1 Representative Brillouin spectra for silica glass at 0.8 GPa and Kilauea basalt glass at 5.9 GPa. Black squares represent raw data while red lines represent Lorentz peak fitting results. At 0.8 GPa, neon is supercritical fluid and only its V_P mode is observed. The Ne back scattering signal marked by * came from the reflected laser on the downstream diamond.

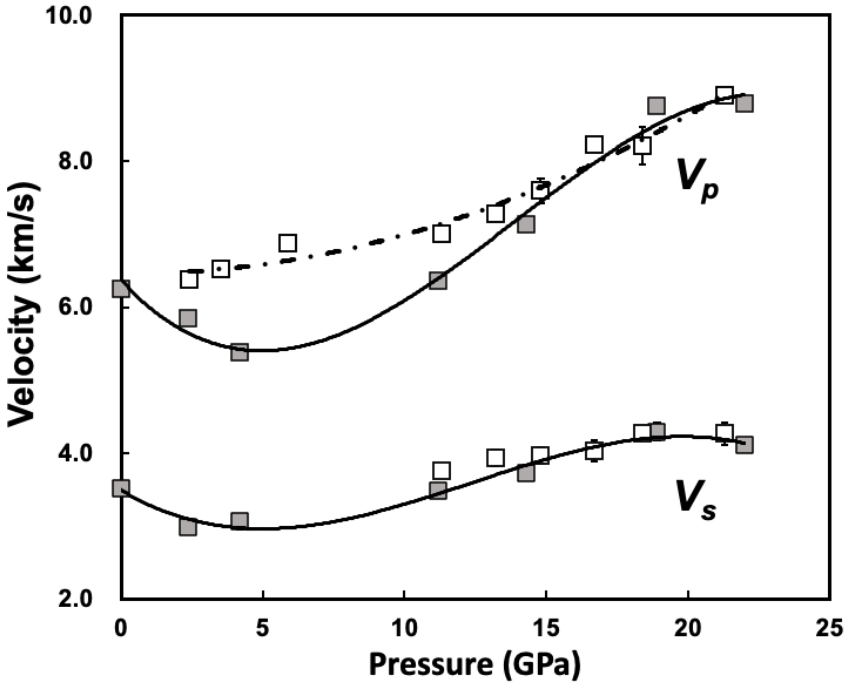

Figure S-2 Compression and decompression measurements of sound velocities of silica glass at high pressure. Filled squares show compression data while open squares show decompression data. Lines are guides for the eye.

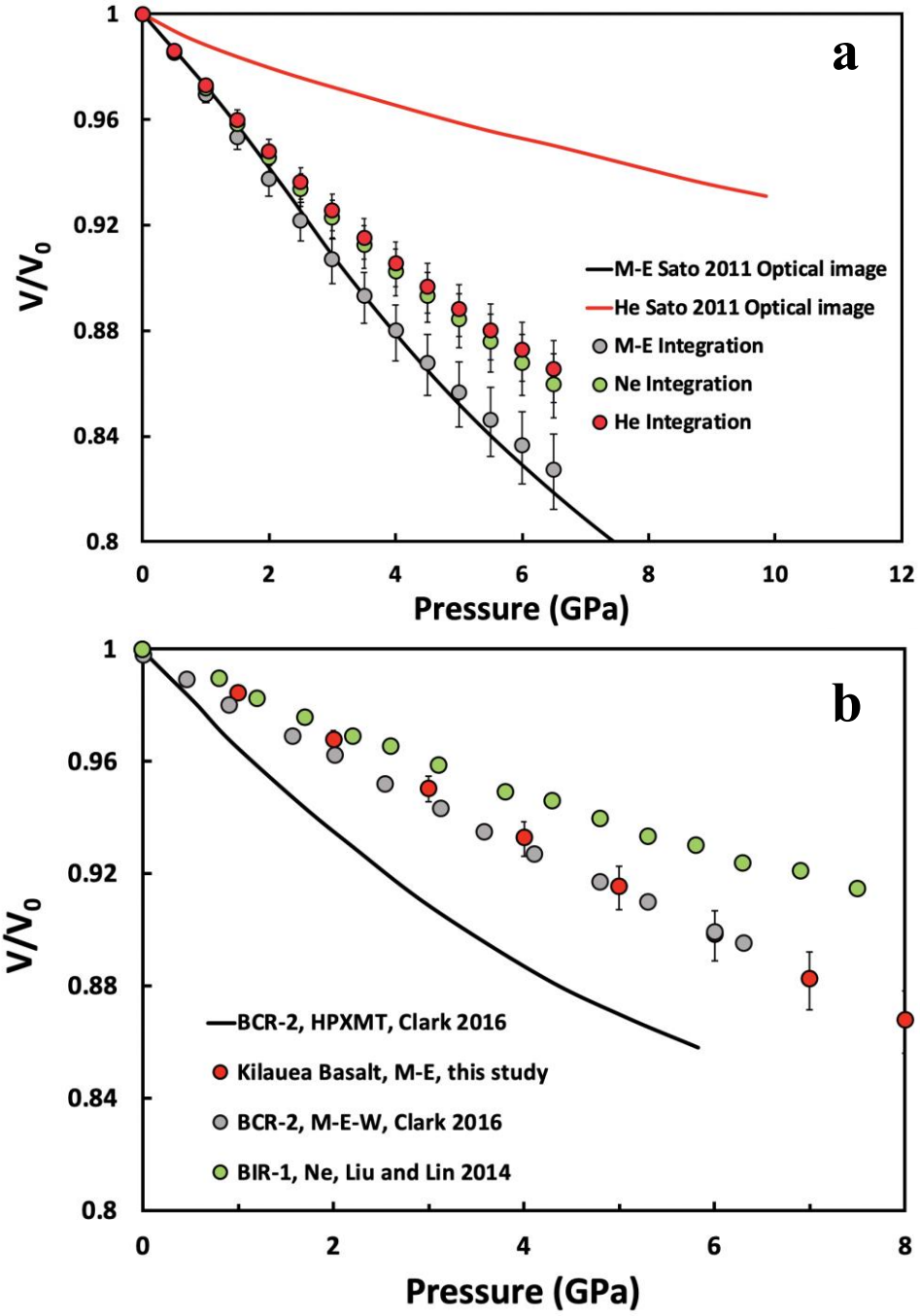

Figure S-3 Relative volume reduction of silica glass and basaltic glasses derived from different methods. M-E-W: 16:3:1 Methanol-Ethanol-Water mixture, M-E: 4:1 Methanol-Ethanol mixture, HPXMT: high-pressure X-ray microtomography. Filled circles are results from bulk sound velocity integration method based on $\frac{V}{V_0} = \left(\frac{\rho}{\rho_0}\right)^{-1} = \left(1 + \frac{1}{\rho_0}\int_{P_0}^{P} \frac{dP}{v_P^2 - \frac{4}{3}v_S^2}\right)^{-1}$ (Eq. S-3). we used a generous ±5% uncertainty in V_S and V_P to calculate the resulting uncertainty in V/V_0. Lines represent results from X-ray tomography (HPXMT) or optical image measurements.

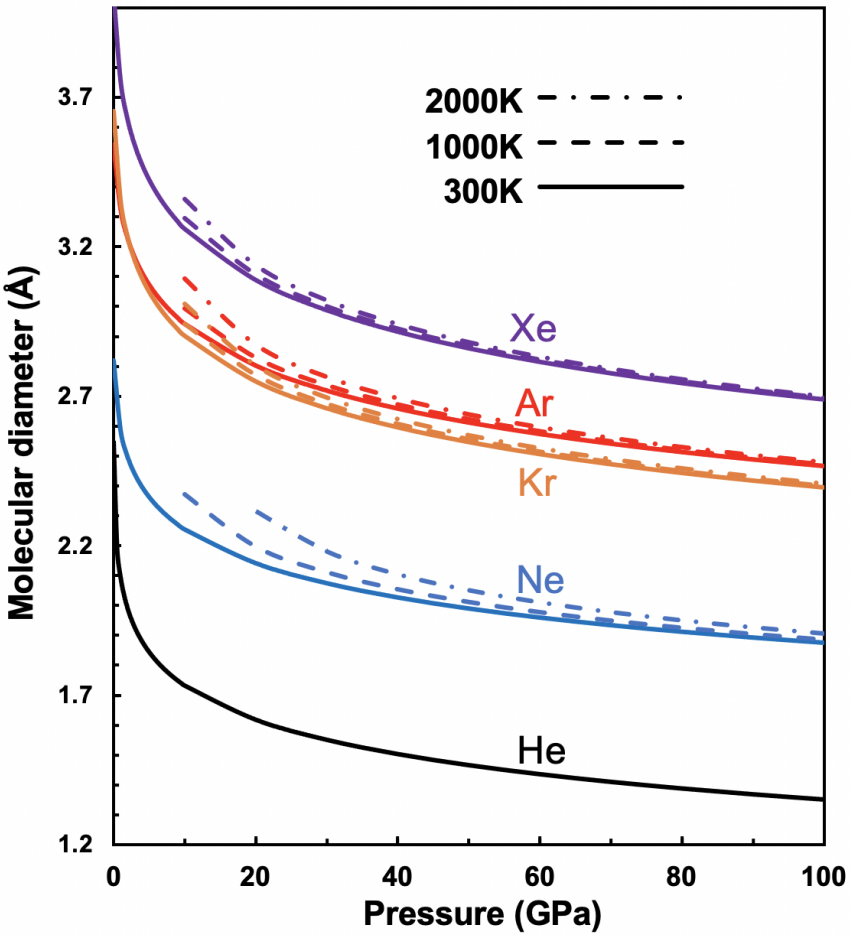

Figure S-4 Molecular size of noble gases as a function of pressure and temperature. Molecular size data at ambient conditions were taken from Reid *et al.* (1987). Thermal EoS data of noble gases were taken from Rosa *et al.* (2020). We did not include the high temperature effect on helium as its thermal EoS above 300 K has not been well established.

Supplementary Information References

Clark, A.N., Lesher, C.E., Jacobsen, S.D., Sen, S. (2014) Mechanisms of anomalous compressibility of vitreous silica. *Physical Review B* 90, 174110.

Clark, A.N., Lesher, C.E., Jacobsen, S.D., Wang, Y. (2016) Anomalous density and elastic properties of basalt at high pressure: Reevaluating of the effect of melt fraction on seismic velocity in the Earth's crust and upper mantle. *Journal of Geophysical Research: Solid Earth* 121, 4232–4248.

Liu, J., Lin, J.-F. (2014) Abnormal acoustic wave velocities in basaltic and (Fe,Al)-bearing silicate glasses at high pressures. *Geophysical Research Letters* 41, 8832–8839.

Jochum, K.P., Dingwell, D.B., Rocholl, A., Stoll, B., Hofmann, A.W., Becker, S., Besmehn, A., Bessette, D., Dietze, H.-J., Dulski, P., Erzinger, J., Hellebrand, E., Hoppe, P., Horn, I., Janssens, K., Jenner, G.A., Klein, M., McDonough, W.F., Maetz, M., Mezger, K., Müker, C., Nikogosian, I.K., Pickhardt, C., Raczek, I., Rhede, D., Seufert, H.M., Simakin, S.G., Sobolev, A.V., Spettel, B., Straub, S., Vincze, L., Wallianos, A., Weckwerth, G., Weyer, S., Wolf, D., Zimmer, M. (2000) The Preparation and Preliminary Characterisation of Eight Geological MPI-DING Reference Glasses for In-Situ Microanalysis. *Geostandards and Geoanalytical Research* 24, 87–133.

Reid, R.C., Prausnitz, J.M., Poling, B.E. (1987) The properties of gases and liquids. McGraw Hill Book Co., New York, NY.

Rivers, M., Prakapenka, V.B., Kubo, A., Pullins, C., Holl, C.M., Jacobsen, S.D. (2008) The COMPRES/GSECARS gas-loading system for diamond anvil cells at the Advanced Photon Source. *High Pressure Research* 28, 273–292.

Rosa, A.D., Bouhifd, M.A., Morard, G., Briggs, R., Garbarino, G., Irifune, T., Mathon, O., Pascarelli, S. (2020) Krypton storage capacity of the Earth's lower mantle. *Earth and Planetary Science Letters* 532, 116032.

Sato, T., Funamori, N., Yagi, T. (2011) Helium penetrates into silica glass and reduces its compressibility. *Nature Communications* 2, 345.

Sinogeikin, S., Bass, J., Prakapenka, V., Lakshtanov, D., Shen, G., Sanchez-Valle, C., Rivers, M. (2006) Brillouin spectrometer interfaced with synchrotron radiation for simultaneous x-ray density and acoustic velocity measurements. *Review of Scientific Instruments* 77, 103905.

Weigel, C., Polian, A., Kint, M., Rufflé, B., Foret, M., Vacher, R. (2012) Vitreous Silica Distends in Helium Gas: Acoustic Versus Static Compressibilities. *Physical Review Letters* 109, 245504.

Whitfield, C.H., Brody, E.M., Bassett, W.A. (1976) Elastic moduli of NaCl by Brillouin scattering at high pressure in a diamond anvil cell. *Review of Scientific Instruments* 47, 942–947.